Texture Analysis Using Local Property Maps

P.P. Smyth, C.J. Taylor and J. Adams
Depts. of Medical Biophysics & Diagnostic Radiology
University of Manchester
pps@wiau.mb.man.ac.uk

Abstract

Morphological granulometry has been shown to be effective in a range of texture analysis applications. We describe an extension to the standard approach which allows truly local properties of the texture to be measured at each pixel. The result is a set of texture features which are analogous to those which could be measured for individual texture primitives, if they could be isolated. We demonstrate the ability of the method to estimate the known properties of the primitives in synthetic texture images and show that reasonably accurate results can be obtained over a range of practically useful conditions. We describe the application of the method to a difficult texture analysis problem - grading the degree of osteoporosis in radiographs of the femoral neck - and show that better results can be obtained than with either Laws' texture features or conventional granulometry.

1 Introduction

Textures are image intensity patterns which normally arise because of the presence of microstructure which cannot be fully resolved. Usually we can think of a texture as being composed of texture primitives. We are often interested in discriminating between natural textures; although these may occasionally be regular and highly predictable, it is much more common to encounter stochastic textures for which there is an element of randomness in both the form of the texture primitives and the way they are placed. Ideally we would characterise each texture by recovering, from the image, a description of the process by which it was generated. Generally this is not possible, so instead we extract statistics which we hope will reflect the nature of the generating process.

Many approaches to texture characterisation have been described. Second order grey-level statistics [1] over a region of interest and methods based on the response to multiple filters [2, 3], again over a region of interest, have proved amongst the most successful of those which have been formally evaluated [4]. More sophisticated filter-based approaches using Gabor functions [5], Wigner distributions [6] or wavelets [7], show promise but have not yet been shown to be superior to simpler methods across a range of texture characterisation applications.

Methods based on mathematical morphology, often known as granulometric methods, have also been found to be effective [8, 9, 10]. The basis of these methods is to 'sieve' out image structures at successively larger scales, evaluating some image metric, such as average intensity over a region of interest, at each scale. The approach is closely related to fractal-based methods [11, 12]. Dougherty [10] suggests making the region of interest a sliding window so that a 'local' characterisation can be obtained for each pixel. Use of the term local is, however, somewhat misleading since the measurements assigned to a pixel have in fact been derived from a window of large, fixed size (e.g. 30x30 pixels).

BMVC 1995 doi:10.5244/C.9.5

If we return to the origins of texture, it seems attractive to try and find methods that work more directly with texture primitives. This is not, however, easy because, as we have already observed, it is generally impossible to isolate individual primitives. The situation is further exacerbated by the fact that, in grey-level images, each pixel may belong to structures at many different scales.

We have investigated a morphological approach to texture characterisation which attempts to obtain truly local structural information over a range of scales; preliminary results were presented previously by Baichoo [13]. The idea is to apply morphological filters to remove successively larger scale structures, recording the changes in grey-level at each pixel rather than over a region of interest. By using directional structuring elements it is possible to obtain length (maximum dimension), width (minimum dimension) and orientation information. These can be combined at the pixel level to give measurements such as aspect ratio which cannot be obtained using region-based methods. Once appropriate local properties have been derived for each pixel, summary statistics can be computed for an area of interest and used for texture classification or segmentation in the normal way.

In the remainder of the paper we give a more detailed explanation of granulometry. We describe our new method and present the results of experiments on synthetic textures designed to test the method's ability to recover the characteristics of known texture primitives in the presence of noise and overlapping structure. We then present results for an experiment in which our method was applied to a real texture analysis problem - grading the degree of osteoporosis from radiographs of the femur - comparing its performance with existing methods.

2 Morphological Granulometry

The basis for morphological granulometry is Matheron's set of axioms relating to the process of obtaining a granulometric size distribution [14]. He describes a 'sieving' transformation $\psi_\lambda(X)$ with parameter λ upon a set X. To use $\psi_\lambda(X)$ to classify members of X on the basis of their value of parameter λ, it must have certain properties. These are

(a) Antiextensivity:
$$\psi_\lambda(X) \subset X \qquad \forall \lambda \geq 0$$
(b) Increasing monotonicity:
$$Y \subset X \Rightarrow \psi_\lambda(Y) \subset \psi_\lambda(X) \qquad \forall \lambda \geq 0$$
(c) Idempotence:
$$\psi_\mu(\psi_\lambda(X)) = \psi_\lambda(\psi_\mu(X)) = \psi_{Sup(\lambda,\mu)}(X) \qquad \forall \lambda, \mu \geq 0$$

Morphological opening is such a sieving process. It combines an erosion followed by a dilation, using a given structuring element, to eliminate all bright structures smaller in size than the structuring element. It obeys Matheron's axioms when one considers X as the set of structures (of varying sizes) in an image, and $\psi_\lambda(X)$ as the opening process at scale λ. Opening can be applied to both binary and greyscale images; in the case of greyscale images, the presence of structure at a scale has an associated value corresponding to the contrast at that scale, rather than merely its presence or absence.

Closing is the dual of opening. It eliminates dark structures of less than the structuring element size. Because we cannot, in general, know whether dark or bright structures are more significant, opening and closing are often used together.

Granulometric methods can employ any structuring element design, although the most easily understood results are obtained using simple (e.g. circular, linear or rectangular) structuring elements. Having obtained a sequence of opened images $I(\lambda)$ for increasing scale λ, some summary statistics are calculated. The mean brightness of $I(\lambda)$

over a region of interest describes the amount of structure $\psi(\lambda)$ still present at scales λ and greater. A size distribution, or local pattern spectrum, $\Phi(\lambda)$, can be derived from $\psi(\lambda)$. This is given by

$$\Phi(\lambda) = \frac{\mathrm{d}}{\mathrm{d}\lambda}\left(1 - \frac{\Phi(\lambda)}{\Phi(1)}\right)$$

Directional opening is a special form of opening, obeying Matheron's axioms. Line-like structuring elements are used to extract lengths and widths of image structures. To perform directional opening at scale λ, the image is opened using structuring elements with a range of orientations. The orientation resulting in the least brightness loss *at each pixel* is selected, and the opened value in that direction is assigned to the directionally opened image. Each pixel therefore has an associated direction at each scale. A linear structure in the image is only eliminated at a particular scale if its longest dimension (length) is less than the length of the linear structuring element at that scale; the brightness loss is a measure of the contrast of the eliminated structure and the direction is an indication of its orientation. Similarly, by selecting the direction resulting in the largest brightness loss, one can perform local width (minimum dimension) sieving; the effect is identical to isotropic opening using a circular structuring element.

3 Local Property Maps

We introduce Local Property Maps which are intended to provide a description of structure in the locality of each pixel. Directional opening is applied at a range of scales giving a series of *length images* $L(\lambda)$; a series of *width images* $W(\lambda)$ are also obtained by simulating isotropic opening as described above. The change in grey-level at each pixel in L and W as a function of λ provides a very rich description of local structure. In the experiments described below we have summarised this information by computing a weighted mean length, width and orientation at each pixel:

$$\begin{aligned}
\text{mean length } \bar{l} &= \sum_{i=1}^{n}[L(\lambda_{i-1}) - L(\lambda_i)]\lambda_i \\
\text{mean width } \bar{w} &= \sum_{i=1}^{n}[W(\lambda_{i-1}) - W(\lambda_i)]\lambda_i \\
\text{mean direction } \bar{\theta} : e^{2i\bar{\theta}} &= \sum_{i=1}^{n}[L(\lambda_{i-1}) - L(\lambda_i)]e^{2i\theta_i}
\end{aligned}$$

where θ_i is the orientation at scale λ_i, and $0 \leq \theta_i < \pi$. An example of an $\bar{l}$ local property map is shown in Figure 1. An important point to note is that the same property value is generally recorded at every pixel in each texture primitive. Given these raw local property maps, additional maps of quantities such as aspect ratio ($\bar{l}/\bar{w}$) and area ($\bar{l} * \bar{w}$) can also be computed. In our experiments so far we have only used opening; a more complete scheme would compute similar properties using directional closing. Once a set of local property maps have been obtained, texture characteristics for a region of interest can be obtained by forming histograms of local property values. The fact that the same property value is measured at every pixel within a given primitive, means that these histograms represent the distribution of local structure in a particularly straightforward way. The histograms are similar to those which would have been obtained for texture primitives if we had been able to isolate them. A number of weighting schemes can be used in forming the histograms - the simplest, a number-of-pixels weighting, is not particularly useful because local properties are only well-defined at pixels where there is

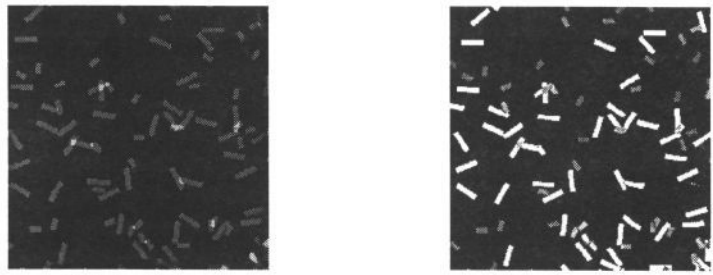

Original image. *Mean length map.*

Figure 1: *A mean length local property map.*

significant local contrast (i.e. where there is significant loss of grey-level intensity over the full range of scales used). Weighting the contribution of each pixel by its local contrast is equivalent to weighting each texture primitive by (contrast*area). A weighting for the contribution of each pixel of (contrast/$(\bar{l} * \bar{w})$) is equivalent to weighting each *texture primitive* by its contrast - given primitives of similar contrast, these two schemes give *area* and *number-of-objects* weighting respectively. Similarly, *length* and *aspect-ratio* weighting schemes can be defined.

4 Experiments with Synthetic Textures

We have used synthetic texture images to test the ability of the methods described above to recover the properties of texture primitives. The synthetic images were generated by placing bright rectangular primitives at random positions and orientations on a dark background. The distributions of lengths, widths and orientations, the density of primitives, and the standard deviation of additive noise could all be varied. Examples of the test images are shown in Figure 2. Values obtained from weighted local property histograms were compared to the known values. In each case, simple distributions of actual texture primitive property values were used so that comparable values could be obtained by taking the means and standard deviations of weighted local property histograms.

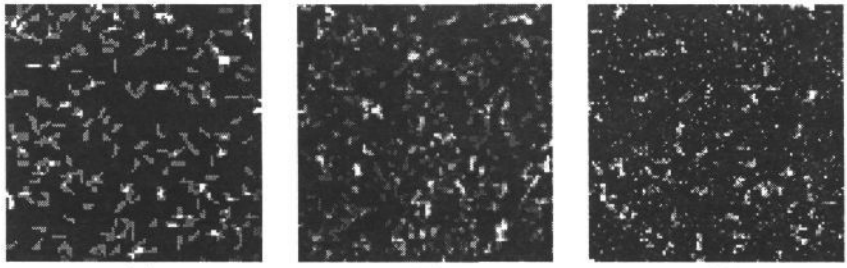

(a) (b) (c)

Figure 2: *Example test images of rectangles size 2x6 pixels. (a): low density (0.2 pixel/pixel), no noise; (b): High density(1.6 pixels/pixel); (c): low density (0.2 pixel/pixel), noise s.d. equal to object brightness.*

4.1 Varying Primitive Density and Noise

Test images were first generated using primitives of fixed size (2x6 pixels) at a relatively low density (0.2 pixel/pixel) to show the behaviour of various weighting schemes. Mean length, width, area and aspect ratio were measured from local property histograms of the images, using length, area, aspect ratio and number-of-objects weighting schemes. Object density and standard deviation of additive noise were then varied. Results for

mean length are shown in Figure 3; similar results were obtained for mean width, mean area and mean aspect-ratio. At relatively low densities all weighting schemes except for number-of-objects weighting gave good results. As primitive density increased, and with it the number of overlaps, the measured mean length increased, which is expected since overlapping primitives can mimic larger primitives. The degradation in performance is, however, graceful, and reasonably good estimates are obtained over a large range of densities. It should be noted that density values of 0.8 and over imply extremely densely packed images.

As the noise standard deviation is increased, relative to the intensity of the primitives, structures become fragmented and appear smaller. In fact the size distribution at each pixel becomes typically bimodal with one mode at small scales due to noise, and a second reflecting the true primitive size; the average of the two distributions decreases as noise is increased. Again, the degradation is relatively graceful and all weighting schemes, except for number-of-objects weighting, are reasonably good. We show later how the effects of noise can be reduced.

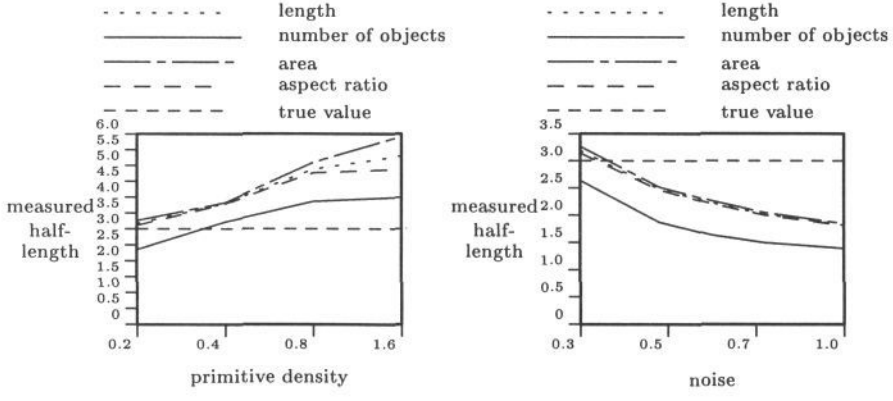

Figure 3: *Measured mean length using various weighting schemes for (left) no noise and increasing primitive density (in pixels/pixel) and (right) fixed primitive density (0.2 pixels/pixel) and increasing noise standard deviation/primitive intensity.*

4.2 Varying the Distribution of Orientations

Test images were created using longer, fixed size rectangles (2x10 pixels), with variable standard deviation of the orientation distribution. The standard deviations of orientations obtained from weighted local property histograms were compared to the known values for various combinations of primitive density and noise standard deviation. Results obtained using area-weighted histograms are shown in Figure 4. There is a reasonably good correspondence between measured and true values over a range of primitive densities, particularly for larger values of orientation s.d. The effect of overlaps leads to over-estimation of the angular dispersion when it is low. Orientation estimates degrade quite rapidly with increasing noise as fragmented structures appear to become more randomly aligned.

4.3 Varying the Distribution of Lengths

Test images were created using primitives of width 5 pixels with lengths between 5 and 20 pixels. Mean lengths obtained from weighted local property histograms were compared to the known values for various combinations of primitive density and noise standard deviation. The results obtained using area-weighted histograms are shown in Figure 5. There is a linear relationship between measured and true length over a range of density

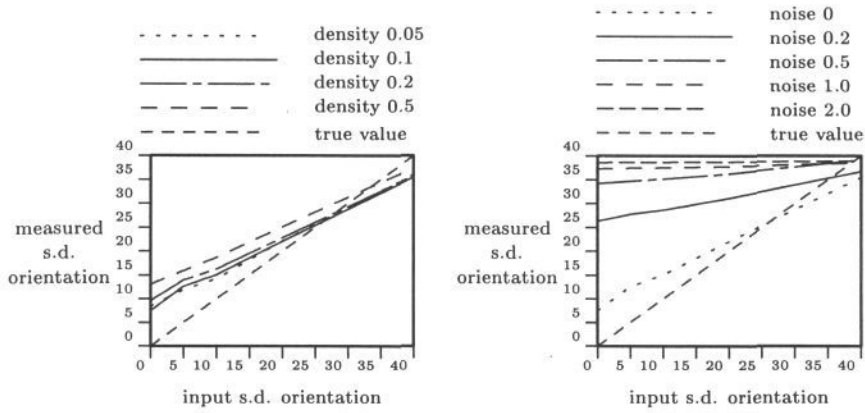

Figure 4: *Measured area-weighted orientation standard deviation (in degrees) against input orientation standard deviation for (left) no noise and various primitive densities (pixels/pixel) and (right) fixed primitive density (0.05 pixels/pixel) and various values of noise standard deviation/primitive intensity.*

and noise conditions, though the absolute errors increase rapidly with noise. Similar results were obtained for mean width, mean area, and mean aspect-ratio. The noise

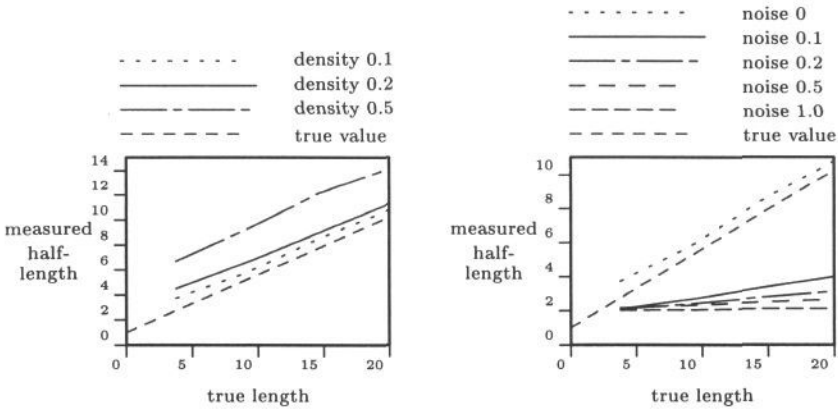

Figure 5: *Measured area-weighted mean length against true length (in pixels) for (left) no noise and various primitive densities (pixels/pixel) and (right) fixed primitive density (0.1 pixels/pixel) and various values of noise standard deviation/primitive intensity.*

experiments were repeated, but with the contribution from the lowest scale (± 1 pixel) excluded from the calculation of the local average property values. The logic behind this was to try reduce the effect of the bimodal local size distribution which results from the addition of noise. The results obtained using area-weighted histograms are shown in Figure 6. The degradation of performance with noise is now much less severe, suggesting that the modified measurements would be useful over a practical range of noise conditions.

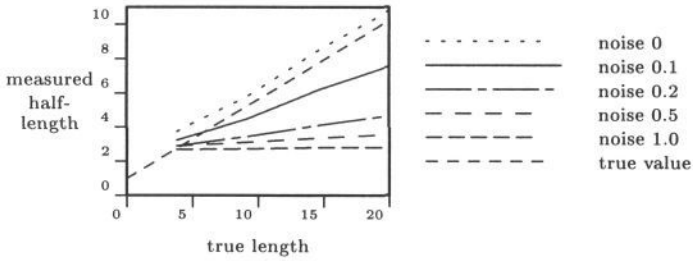

Figure 6: *Measured area-weighted mean length against true length for fixed primitive density (0.1 pixels/pixel) and various values of noise standard deviation/primitive intensity excluding finest scale information.*

4.4 Summary of Results

In summary, mean local property values reflect the known property values of primitives well. The test conditions we used included extremely dense textures and extremely noisy images. Despite this, linear relationships were found between measured and true values over most of the test conditions, with reasonably good absolute accuracy for conditions likely to be met in real applications. Excluding information below a half length of 1 pixel was useful in extending the range of noise conditions over which useful length discrimination could be expected.

5 Application to a Real Texture Problem

Given these encouraging results for synthetic data, we applied our approach to a medical texture analysis problem - grading the degree of osteoporosis from radiographs of the femoral neck. We compared the performance of our new texture features with Laws' spatial filter-based approach and with conventional granulometry using linear structuring elements.

5.1 Grading Degree of Osteoporosis

Osteoporosis is a condition characterised by a loss of bone, and is a major cause of hip and vertebral fractures. As bone is lost, thin load-bearing trabecular structures become reduced in number, length and thickness, weakening the femoral neck as a whole and increasing the likelihood of fracture. One standard manual method of assessing the likelihood of a hip fracture from osteoporosis is the Singh index [15], performed by describing the texture of the trabeculae over a few key regions in the neck of the femur, imaged using standard radiography. Example radiographs of normal and osteoporotic cadaver femora are shown in Figures 7 & 8. It would be desirable to develop an automated method of assessing the degree of osteoporosis reliably from these images. The task of ranking femora according to degree of osteoporosis is one which radiologists find difficult, and is a challenging texture analysis problem. For reproducible assessments, repeated measurements by more than one radiologist are required. Automation of this task using computer vision would potentially improve the consistency and reduce the cost and time for the assessment. Twenty-five standard radiographs, taken of cadaver femora, were ranked for degree of osteoporosis twice each by two experienced radiologists using Singh's criteria. The examples were known to cover only the range of osteoporosis from normal to moderate, increasing the difficulty of the ranking task. The inter- and intra-correlations of the radiologists' rankings were recorded, and the mean rank for each case was taken as the 'ground truth' for training and testing texture features.

Five regions for performing texture analysis corresponding to those defined by Singh were each marked by a radiologist on the first five examples. The position of these regions

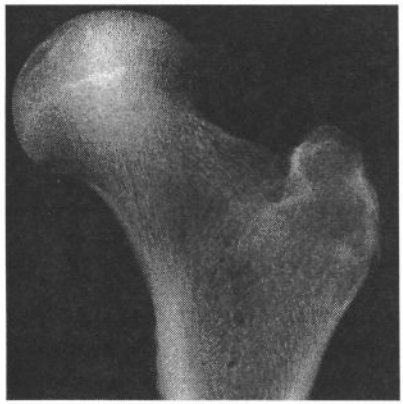

Figure 7: *A normal femur.*

Figure 8: *An osteoporotic femur.*

was described in terms of a coordinate system based upon the centre of the femoral head, and line of narrowest femoral neck cross-section. These anchor points for the coordinate system were then marked on the remaining examples to define the absolute positions of the regions of interest. The regions and coordinate system are shown in Figure 9. In the experiments described here we only used data from region 2, known as Ward's triangle, and recognised as the area most sensitive to bone loss. The integrated grey-level for the region was normalised before further analysis, correcting for the effects of variable film processing and ensuring that only textural properties could be used in the automated task.

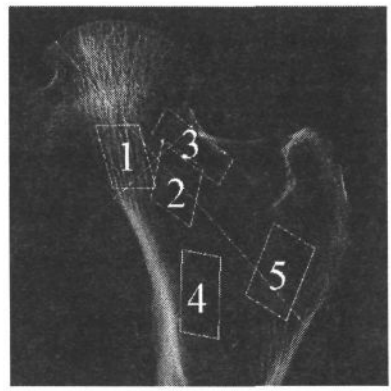

Figure 9: *The five regions of interest, and the coordinate system to position them.*

5.2 Experimental Details

Local feature maps were created for mean length, mean width, mean area, and mean aspect-ratio, using length information in the range 5-51 pixels (excluding the smallest scale) and width information in the range 5-15 pixels. These ranges were chosen to reflect the scales of the structures which are known to disappear as osteoporosis progresses. Area-weighted local property histograms were computed and resampled logarithmically into five bins each. The values in these bins for each of the four property histograms gave a total of 20 texture features. Of these 20 features the 10 length and width features are similar to those obtained using conventional granulometry and were considered separately for comparison. The area and aspect-ratio features are intrinsically local. Laws' texture

features were also computed using 5x5 kernels and normalising by the L5L5 smoothing filter to give 24 texture features [2].

The features were used in a linear regression model to predict rankings for unseen radiographs. The feature values were ranked to transform them from an assumed monotonic to a uniform distribution for use as the independent variables in the regression. We used a leave-one-out methodology, or cross-validation, to avoid an optimistic bias in the assessment of automatic ranking performance, performing training using each subset of 24 examples in turn and testing the performance on the remaining example. Given only 25 examples it was clearly necessary to perform selection from each of the feature sets to avoid overfitting to the design data at the expense of poor performance on unseen examples.

It was necessary to include the feature selection process as part of the leave-one-out training phase, so as to eliminate the (significant) bias inherent in performing feature selection from a large number of variables using all training examples. Otherwise, good results could have been obtained using sets of random numbers rather than real feature measurements. This method is described for linear discriminant analysis by Ganeshanandam & Kryzanowski [16], and was applied here in a similar fashion. The neccesary use of cross-validation made it difficult to calculate confidence intervals for the measured ranking performance in order to test for significance between feature sets. An effective value of Spearman's rank correlation coefficient (R_s(effective)) (taking the ranking based on the radiologists' mean ranks as the true ranking) was computed from the difference sum-of-squares as the measure of ranking performance. The procedure was repeated with values of 1,2,3 and 4 for n.

5.3 Results

The intra-performance of the two radiologists gave values of Spearman's rank correlation coefficients (R_s) of 0.760 & 0.923, and the inter-performance gave $R_s = 0.830$. The performance of the automatic methods, for different values of n, the number of texture features, are shown in Table 1. The performance of the best combination of texture methods was not as good as that of the least consistent radiologist but very much better than random ($R_s = 0.485$ is the 0.01 significance level for a sample of 24). It should be noted, however, that for small samples the leave-one-out approach gave a pessimistic estimate of performance because generalisation from the design set is likely to be unsuccessful when the design set is small. Also our measure of radiologists' performance was slightly optimistic compared to that used for the texture features - we should really have tested independant radiologists against the 'ground truth' ranking produced by our existing experts. Feature selection for the local property method generally resulted in a combination which included a particular length feature and one of two aspect-ratio features. This is consistent with the qualitative interpretation that, as osteoporosis proceeds, structures become thinner, decreasing widths and increasing aspect ratios. The additional information from the uniquely local features leads to the best overall result, though a larger training/test set would be needed to establish statistical significance.

	20 Local measures	10 length/width measures	24 Laws measures
n	R_s(effective)	R_s(effective)	R_s(effective)
1	0.538	0.574	**0.631**
2	**0.667**	0.599	0.516
3	0.601	**0.633**	0.533
4	-	0.439	-

Table 1: *Performance of texture features in ranking 25 radiographs for osteoporosis varying n, the number of features selected.*

6 Conclusions

We have described a new method of texture characterisation which extends existing granulometric methods to give truly local sizing of texture primitives. Results for synthetic texture images show that the method is able to recover the properties of known texture primitives reasonably well over a range of practically useful operating conditions. The approach we have described for extracting local property maps from the multi-scale measurements available at each pixel are somewhat simplistic and it may be possible to improve on the approach. Application of the new method to a real texture analysis problem has produced encouraging results. More extensive testing on a range of texture analysis problems and with larger test sets is required.

References

[1] Haralick RM, Shanmugam K and Dinstein I, *Textural features for image classification.* IEEE Transactions on Systems, Man and Cybernetics, 3, 1973, pp 610-621.

[2] Laws KI, *Textured Image Segmentation.* Technical Report USCIP Report 940, Dept of Elec. Eng., Image Processing Institute, Univ. of Southern California, Los Angeles, 1980.

[3] Unser M, *Local linear transforms for texture measurements.* Signal Process., 11, 1986, pp 61-79.

[4] duBuf JMH, Kardan M, and Spann M, *Texture feature performance for image segmentation.* Pattern Recognition 23, 1990, pp 291-309.

[5] Turner MR, *Texture Discrimination by Gabor functions.* Biol. Cybernet., 55, 1986, pp 71-82.

[6] Knutson H and Granlund GH, *Texture analysis using two-dimensional quadrature filters.* IEEE Workshop CAPAIDM, Pasadena, CA, 1983, pp 206-213.

[7] Reed TR and Wechsler H, *Tracking of non-stationarities for texture fields.* Signal Process., 14, 1, 1988, pp 95-102.

[8] Peleg S, Naor R, Hartley R and Avnir D, *Multiple resolution texture analysis and classification.* IEEE Trans. Pattern Anal. Mach. Intell., 6, 1984, pp 518-523.

[9] Jasiobedski P, Taylor CJ and Brunt JNH, *Automated analysis of retinal images.* Image and Vision Computing, 11, 1993, pp 139-144.

[10] Dougherty ER, Newell JT and Pelz JB, *Morphological texture-based maximum-likelihood pixel classification based on local granulometric moments.* Pattern Recognition, 25, 10, 1992, pp 1181-1198.

[11] Pentland AP, *Fractal-based description of natural scenes.* IEEE Trans. Pattern Anal. Mach. Intell., 6, 1984, pp 661-674.

[12] Keller JM, Chen S and Crownover RM, *Texture description and segmentation through fractal geometry.* Computer Vision Graphics and Image Processing, 45, 1989, pp 150-166.

[13] Baichoo, *Texture analysis of the microscopic structure of wound tissue.* MSc thesis, 1993, University of Manchester.

[14] Matheron G, *Random Sets and Integral Geometry.* Wiley, New York, 1975.

[15] Singh M, Nagrath AR, and Maini PS, *Changes in trabecular pattern of the upper end of the femur as and index of osteoporosis.* J Bone Joint Surg., 52A, 1970, p 437.

[16] Ganeshanandam S and Kryzanowski WJ, *On selecting variables and assessing their performance in linear discriminant analysis.* Austral. J. Statist., 31(3), 1989, pp 433-447.